

Supporting Information

Highly Efficient Solar Steam Generation from Activated Carbon Fiber Cloth with Matching Water Supply and Durable Fouling Resistance

Qile Fang^{a,b,†}, Tiantian Li^{a,b,†}, Haibo Lin^{a,b}, Rongrong Jiang^a and Fu Liu^{a,b,}*

^aKey laboratory of Marine Materials and Related Technologies, Zhejiang Key Laboratory of Marine Materials and Protective Technologies, Ningbo Institute of Materials Technology & Engineering, Chinese Academy of Sciences, No. 1219 Zhongguan West Rd, Ningbo, 315201, China

^bUniversity of Chinese Academy of Sciences, 19 A Yuquan Rd, Shijingshan District, Beijing, 100049, China

Corresponding Author

* E-mail: fu.liu@nimte.ac.cn (Fu Liu)

The SI file includes:

Table S1. The corresponding properties of ACFC

Figure S1. SEM image of the cotton fiber non-woven fabrics (CFNF)

Figure S2. The relationship of evaporation and water transport rate on the surface of solar steam generation system when ACFC combined with different layers of CFNF.

Figure S3. The ion concentrations before and after solar desalination using ACFC+4

Figure S4. Mass change of natural water evaporation at experiment condition (without sun illumination)

Calculation of solar-steam conversion.

Heat loss analysis

Figure S5. The surface temperature and its adjacent environment temperature of ACFC+4 under one sun illumination

Table S2. Summarization of evaporation rate and conversion efficiency of light-thermal materials

Figure S6. Mass change of salt water during a long time illumination (12h) under one sun

Figure S7. Conductivity of the bulk water (3.5% NaCl, 80 mL) after salt infiltrating back via ACFC and ACFC+4 during 110 min as shown in Figure 5e, Control: 3.5% NaCl solution, Control+NaCl: 80 mL 3.5% NaCl solution + 0.5 g solid NaCl

Table S1. The corresponding properties of ACFC

Filament diameter (μm)	Ignition point ($^{\circ}\text{C}$)	Ash content (%)	Bulk density (g cm^{-3})	Specific area ($\text{m}^2 \text{g}^{-1}$)	Pore volume ($\text{cm}^3 \text{g}^{-1}$)	Pore size distribution (%)			
						<1 nm	1-2 nm	2-5 nm	>5 nm
10~20	> 500	2~3	0.04~0.1	800~1800	0.9~1.28	83~84	6~7	6~7	4~5

*The data was provided by the supplier of ACFC

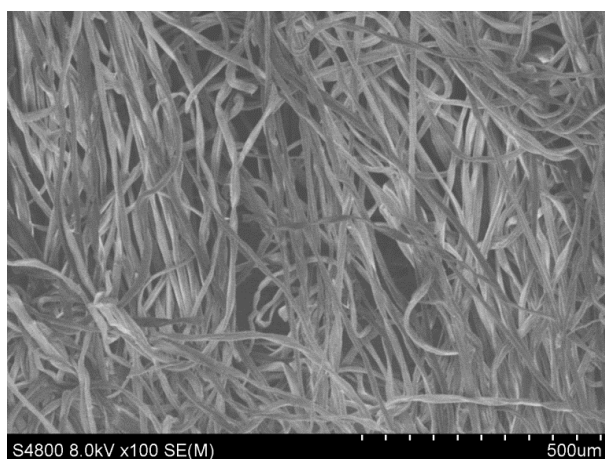


Figure S1. SEM image of the cotton fiber non-woven fabrics (CFNF)

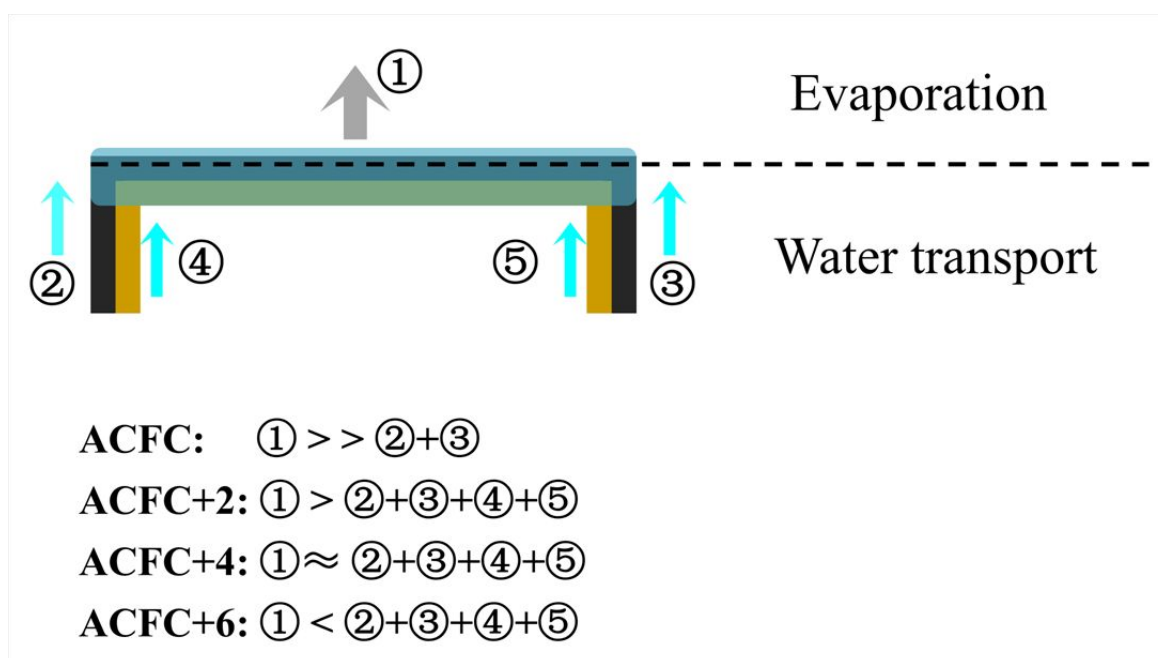


Figure S2. The relationship of evaporation and water transport rate on the surface of solar steam generation system when ACFC combined with different layers of CFNF.

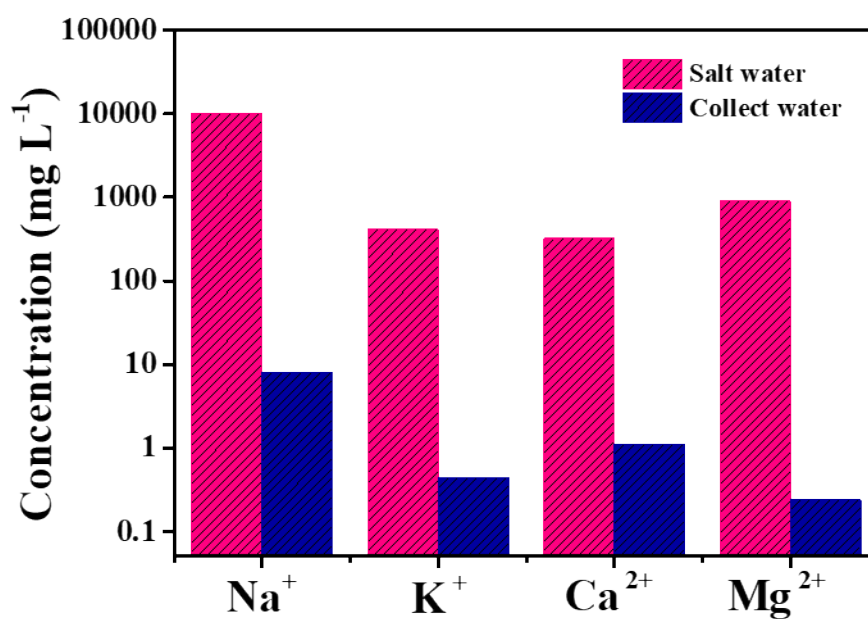


Figure S3. The ion concentrations before and after solar desalination using AFCF+4

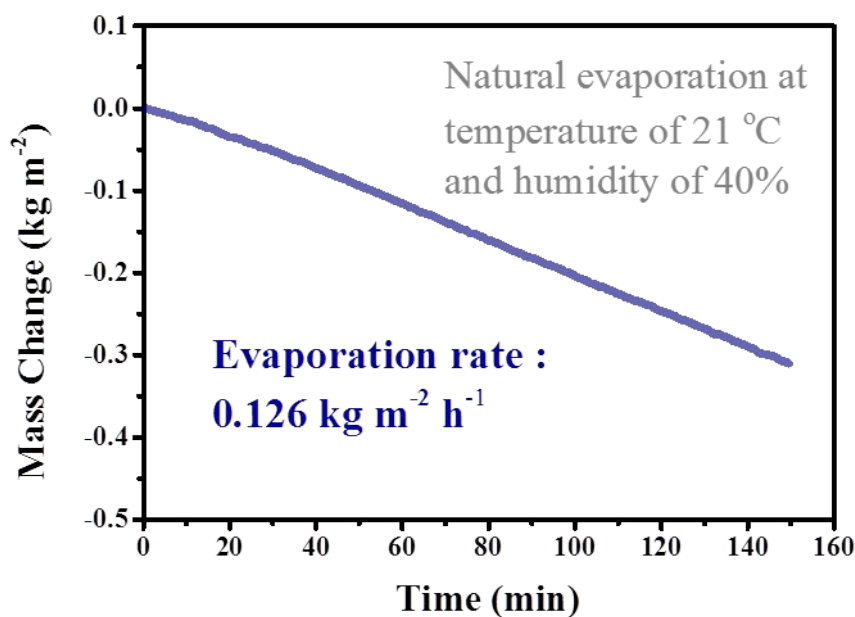


Figure S4. Mass change of natural water evaporation at experiment condition (without sun illumination)

Calculation of solar-steam conversion.

The conversion efficiency is calculated by

$$\eta = m h_{lv} / P_{in}$$

where η is solar-steam conversion efficiency, m is the mass flux of steam, h_{lv} denotes the total enthalpy, including the liquid-vapor phase change enthalpy (2260 J g⁻¹) and the sensible heat, and P_{in} is the solar illumination energy. The natural evaporation of pure water without sun illumination (0.126 kg m⁻² h⁻¹, Figure S3) has been considered and subtracted from all the measured evaporation rates to calculate the conversion efficiency.

Heat loss analysis

In the interfacial solar steam generation system, the localized thermal energy at ACFC surface via light-thermal conversion is divided into four parts: evaporation, radiation, convection, and conduction, and the latter three constitute the heat loss of the system. The detailed calculation of heat loss is illustrated below.

Radiation

Stefan-Boltzmann equation is used to calculate the radiation loss

$$\Phi = A\varepsilon\sigma(T_1^4 - T_2^4) \quad \text{Equation S1}$$

where Φ is the heat flux, A the surface area of the absorber used in the system ($2 \text{ cm} \times 2.5 \text{ cm}$), ε the emittance of the absorbing surface (0.97), σ the Stefan-Boltzmann constant ($5.6703 \times 10^{-8} \text{ W m}^{-2} \text{ K}^{-4}$), T_1 is the surface temperature of ACFC under one sun illumination (31.6°C), T_2 is the adjacent environment temperature (28°C). The radiative heat loss is 22.0 W m^{-2} .

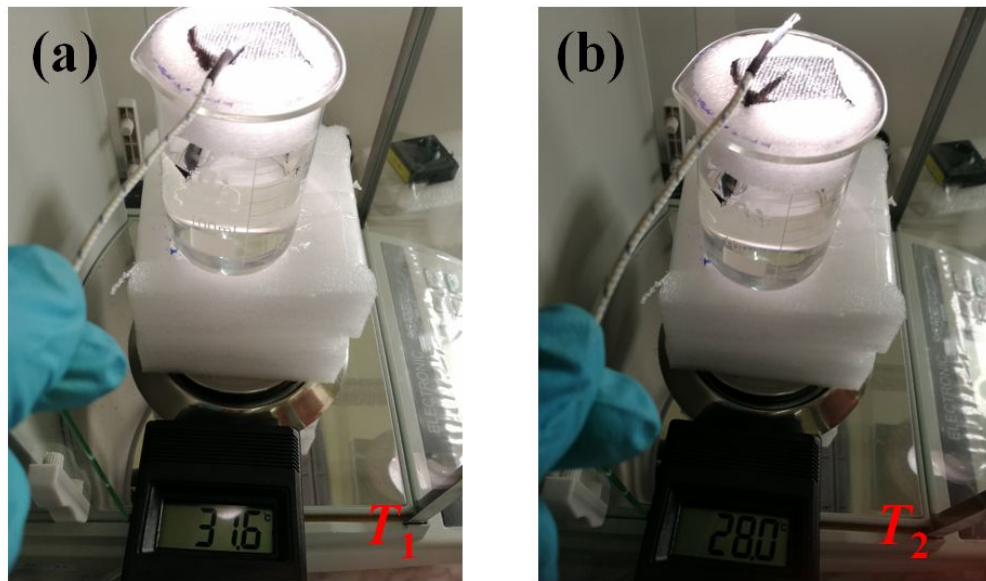


Figure S5. The surface temperature and its adjacent environment temperature of ACFC+4 under one sun illumination

Convection

Equation S2 based on Newton' law of cooling is used to calculate the convection of heat loss

$$Q=Ah(T_1-T_2) \quad \text{Equation S2}$$

where Q is the heat flux, A the surface area of the absorber used in the system (2 cm × 2.5 cm), h the natural convection heat transfer coefficient (10 W m⁻² K⁻¹) (*Nat. Energy*, **2016**, 1, 126), T_1 is the surface temperature of ACFC under one sun illumination (31.6 °C), T_2 is the adjacent environment temperature (28 °C). The convective heat loss is 36.0 W m⁻².

Conduction

Although PS foam and air gap are set as thermal insulation layer in the interfacial solar steam generation system, a portion thermal loss conducted to bulk water might occur via the side water path of ACFC. Equation S3 is used to calculate the heat loss of conduction

$$Q=Cm\Delta T \quad \text{Equation S3}$$

where Q is the heat flux, C the specific heat capacity of water (4.2 kJ °C⁻¹ kg⁻¹), m the bulk water weight used in the experiment (80 g), ΔT the temperature change of the bulk water with insulation installation after evaporation within 1h (0.05 °C, the sensitivity of thermoelectric thermometer is 0.1°C, and there were no dection of temperature change within 1h, but 0.1 °C increase after 2h). The conduction heat loss is 9.3 W m⁻².

Therefore, the total heat loss is 67.3 W m⁻², 6.7% to the input solar energy.

Table S2. Summarization of evaporation rate and conversion efficiency of light-thermal materials

Light-thermal materials	Optical concentration	Evaporation rate (kg m ⁻² h ⁻¹)	Efficiency (%)	References
Graphene oxide film with 2D water path	1	1.45	80	[3]
Thin-film black gold membrane	1	0.67	47	[4]
Al nanoparticles -3D porous membrane	4	5.7	88.4	[6]
Black amorphous Al-Ti-O nanostructure	1	1.03	64.46	[7]
TiAlON-based nanocomposite with A 1D water supply channel	1	1.13	73	[15]
N-doping 3D porous graphene	1	1.5	80	[20]
Bilayer wood with a carbonized surface	1	~1	57.3	[21]
Carbonized mushrooms	1	1.475	78	[22]
3D printing all-in-one evaporator with GO/CNT/NFC	1	1.25	85.6	[24]
Flexible wood/CNTs membrane	1	0.95	65	[25]
	3	2.88	67	
	5	5.14	72	
Narrow-bandgap Ti ₂ O ₃ nanoparticles	1	1.32		[26]
	5	5.03		
Graphene oxide-based evaporator with 1D water path	1	1.27	87.5	[27]
Functionalized graphene with hydrophilic groups	1	0.47	48	[37]
GO-SA-CNT aerogels	1	1.622	83	[38]
Black titania with unique nanocage structure	1	1.13	70	[39]
Black TiO _x nanoparticles	1	0.8012	50.3	[40]
Narrow-bandgap Ti ₂ O ₃ nanoparticles	1	1.32		[41]
	5	5.03		
Monolithic polymer foam	1	1.1687	80.5	[42]
Non-stoichiometric MoO _{3-x} quantum dots	5	4.95	62	[43]
CNT modified filter paper	1	1.1	73	[44]
Polydopamine-filled bacterial nanocellulose	1	1.13	78	[45]
	3	3.47	82	
Coke-derived carbons	2	1.85	62.8	[46]
Fe ₃ O ₄ @C film	1	1.03		[47]
ACFC+CFNF	1	1.59	91.8	This work
	2	2.80	83.7	
	3	3.99	80.5	
	4	5.58	86.2	
	5	7.29	89.0	

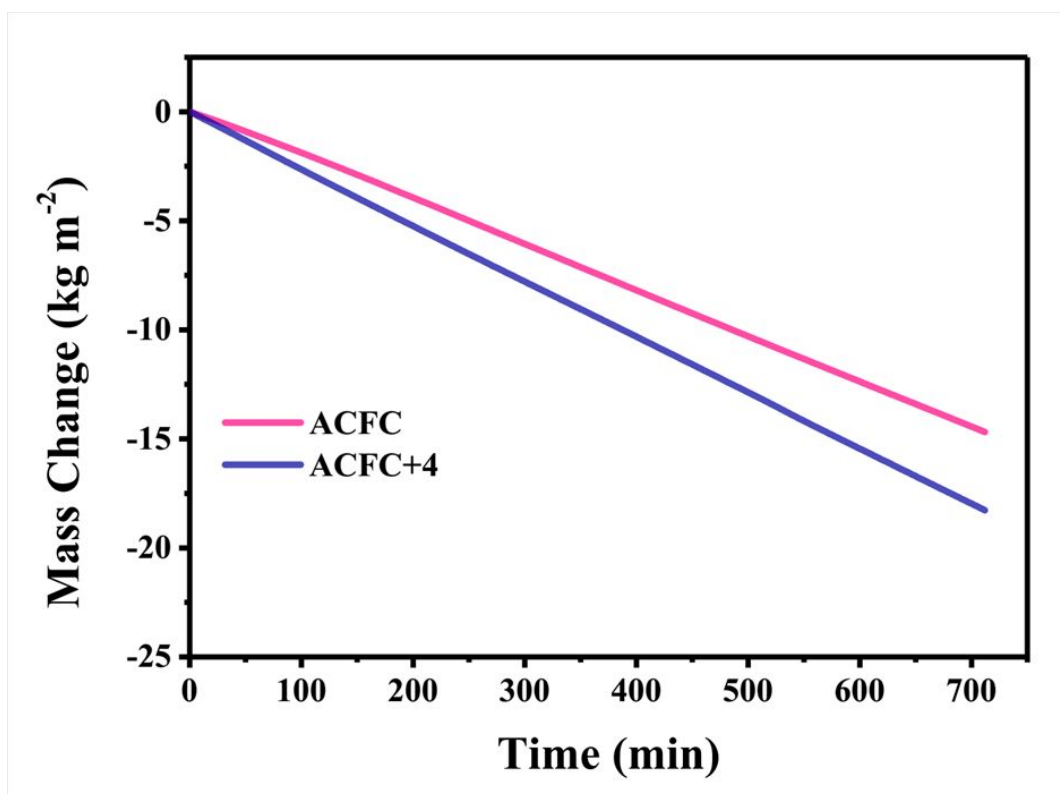


Figure S6. Mass change of salt water during a long time illumination (12h) at one sun

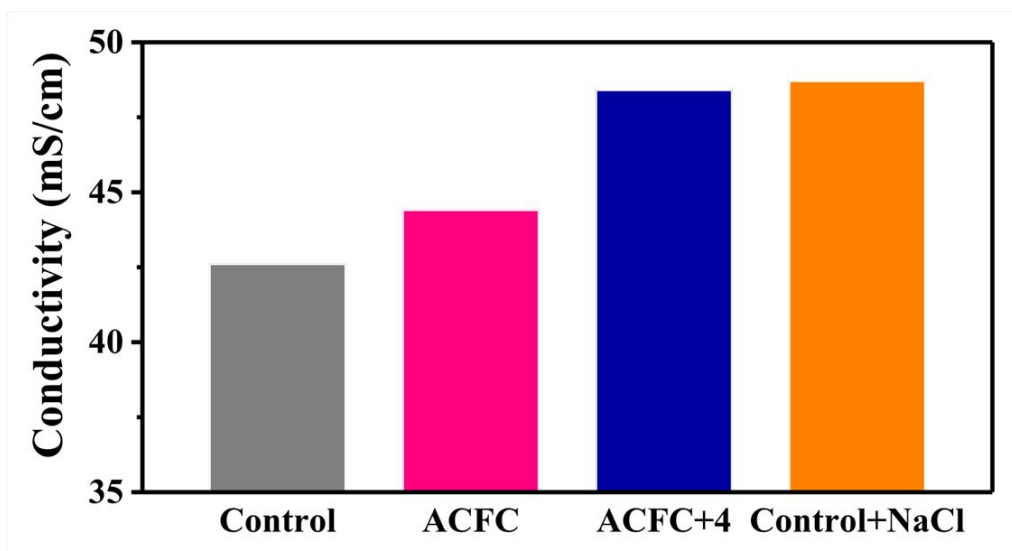


Figure S7. Conductivity of the bulk water (3.5% NaCl, 80 mL) after salt infiltrating back via ACFC and ACFC+4 during 110 min as shown in Figure 5e, Control: 3.5% NaCl solution, Control+NaCl: 80 mL 3.5% NaCl solution + 0.5 g solid NaCl.